

Wideband THz Multi-User Downlink Communications with Leaky Wave Antennas

Yaela Gabay, Nir Shlezinger, *Senior Member, IEEE*, Tirza Routtenberg, *Senior Member, IEEE*, Yasaman Ghasempour, George C. Alexandropoulos, *Senior Member, IEEE*, and Yonina C. Eldar, *Fellow, IEEE*

Abstract—Future wireless systems are envisioned to utilize the large spectra available at THz bands for wireless communications. Extremely massive multiple-input multiple-output (MIMO) antennas can be costly and power inefficient for wideband THz communications. An alternative antenna technology, which can achieve low cost and power efficient THz signaling, is based on leaky wave antennas (LWAs). In this paper, we explore the usage of the LWAs for wideband downlink multi-user THz communications. We propose a model for LWA-aided communication systems that faithfully captures the antenna operations. We show that LWAs yield frequency-dependent beams, where the equivalent wideband channel induces dependence between angle, frequency, and spectral lobe width. We identify the LWA's inherent frequency-selective beamsteering capabilities as motivating multi-band THz communications that deviate from conventional orthogonal frequency-division, and employ non-identical subbands. Then, we propose an alternating optimization algorithm for jointly optimizing the LWA configuration along with the spectral division and power allocation to maximize the achievable sum-rate. Our numerical results show that a single LWA can generate diverse beampatterns, exhibiting performance comparable to costly fully digital MIMO. Interestingly, we demonstrate that allowing transmission with non-identical subbands leverages the characteristics of LWA-based channels compared to uniform division, yielding improved beamsteering that translate to higher rates

I. INTRODUCTION

Wireless communications are subject to constantly growing demands in throughput, connectivity, and latency [2]. To meet these requirements, future wireless systems will utilize high-frequency regimes, and particularly explore the abundant bandwidth available at THz bands [3], [4]. Indeed, the exploration of such wide bandwidth is expected to overcome the spectral congestion of legacy bands [5], [6], and support the throughput requirements of the upcoming sixth generation (6G) wireless technologies [7].

Parts of this work were presented at the IEEE International Conference on Acoustics, Speech, and Signal Processing (ICASSP) 2024 as the paper [1]. Y. Gabay, N. Shlezinger, and T. Routtenberg with the School of ECE, Ben-Gurion University of the Negev, Israel (e-mail: yaelag@post.bgu.ac.il; {nirshl; tirzar}@bgu.ac.il). Y. Ghasempour is with the Department of ECE, Princeton University, NJ, USA (e-mail: ghasempour@princeton.edu). G. C. Alexandropoulos is with the Department of Informatics and Telecommunications, National and Kapodistrian University of Athens, 15784 Athens, Greece and the Department of Electrical and Computer Engineering Department, University of Illinois Chicago, Chicago, IL 60601, USA (e-mail: alexandg@di.uoa.gr). Y. C. Eldar is with the Faculty of Math and CS, Weizmann Institute of Science, Rehovot, Israel (e-mail: yonina@weizmann.ac.il).

This work was partially supported by the Israeli Ministry of National Infrastructure, Energy, and Water Resources, the SNS JU project TERRAMETA under the European Union's Horizon Europe research, innovation programme under Grant Agreement No 101097101, and the US National Science Foundation under Grant Number CNS-2145240.

Despite the promising spectral resources that can be provided by THz bands, designing communication systems that operate in such high frequencies induces critical design challenges in terms of hardware, power, and energy efficiency. Consequently, THz systems are likely to deviate from conventional fully digital multiple-input multiple-output (MIMO) antenna architectures employed in, e.g., legacy sub-6 GHz bands [8]. Such traditional architectures, comprised of multiple antenna elements, each connected with a dedicated RF chain, are expected to be extremely costly in THz bands [9].

To date, several different architectures for THz systems are considered in the literature. A common approach assumes hybrid analog/digital MIMO transceivers [10]–[14]. However, these architectures typically rely on phase shifters [15], which can be limiting factors in terms of power consumption and frequency dependence in THz bands. Additionally, for a multi-user multi-carrier THz communication system, there are strict limitations over the number of directed beams that can be formed simultaneously by a given number of antennas in traditional arrays. Thus, the angular range of a specific fixed antenna configuration is limited. A related family of approaches implements antennas using metasurfaces [16]–[20], possibly as a form of holographic MIMO [21]. However, such architectures are typically not designed for wideband THz signaling and have been primarily conceptually studied for the narrowband case [22].

Another emerging architecture is based on true-time-delay (TTD) circuitry in hybrid MIMO, either replacing phase shifters [23] or in addition to them [24]–[28]. Such architectures can create several on-demand frequency-dependent beams [29], [30] to serve users at a wide range of angles. Such spatially spectral beams are fundamentally different from small dispersion effects (known as beam squint) in traditional phased arrays, which are usually regarded as unwanted side effects causing severe array gain loss [24]–[28], [31]. In [26], a TTD-based precoder was presented, realizing improved achievable rates and energy efficiency than hybrid precoding, and [29], [30] proposed a TTD-based system architecture that was matched with an access control protocol, synchronizing multi-user communications under a fixed beam configuration. While these works indicate the potential gains of exploiting frequency-selective beams in THz regime, the increased cost, hardware complexity, and power consumption associated with numerous phase-shifters and TTDs circuitry required for these architectures hinder their adoption in practical settings.

An alternative emerging antenna technology that is particularly suitable for THz wireless communications is based on

leaky waveguides [32]–[34]. Leaky wave antennas (LWAs) enable frequency-selective beamsteering of extremely wide-band signals [35], creating the so-called THz rainbow [36]. The beampatterns generated by LWAs resemble those produced by hybrid MIMO transmitters utilizing TTD and phase shifters [24]–[28], albeit in a cost and power efficient manner [37]–[39]. Despite their potential for THz communication systems, LWAs are mostly studied in terms of localization [40], [41] and wireless security [42], while their transmission model and ability to support wideband multi-user wireless communications have not yet been studied.

In this work, we consider LWA-aided THz communications focusing on multi-user downlink systems. We propose a transmission model for LWA signaling that enables exploring their beamforming capabilities for multi-user communications, while faithfully capturing the antenna operations, as physically formulated and experimentally validated in [36]. We identify two design parameters of LWAs: the plate separation and slit length, which directly impact the three-dimensional (3D) angle-frequency relationship, and the resulting frequency-dependent directional beams. Looking into the resulting beampatterns, we identify an inherent lack of symmetry in the induced channel’s behavior towards frequency changes, which motivates us to deviate from conventional orthogonal frequency-division multiplexing (OFDM) and optimize the bandwidth division. We then propose an algorithm based on alternating optimization for jointly tuning the LWA parameters alongside the digital power allocation and spectral division for wideband signaling, with the goal of maximizing the achievable sum rate under physical constraints. We numerically show that a single LWA can form various beampatterns that support multiple downlink users, achieving sum-rate performance that is comparable with fully digital MIMO systems that are equipped with multiple antennas and complex power-demanding phase shifting/time delay capabilities [43].

Our main contributions are summarized as follows:

- **LWA-aided communication model:** We formulate a physically compliant model for downlink wideband THz communications, where transmission is carried out using an LWA. Our model converts physical characterizations of leaky waveguides into a mathematical model that supports studies from a communications theory perspective.
- **Spectral band adaptation:** Our modeling of LWA-based channels unveils that, unlike conventional MIMO systems, in LWA-induced channels, the coherence bandwidth alters throughout the spectral band. Therefore, the resulting spectral profile is not properly exploited by conventional uniform subband division, as typically employed by OFDM signaling. This observation motivates us to deviate from OFDM into non-uniformly-spaced spectral bands when utilizing LWAs.
- **Transmission and LWA optimization:** We propose an algorithm for jointly optimizing the internal LWA parameters along with the spectral allocation. This algorithm employs alternating optimization on the design parameters, with dedicated tools to tune each parameter, and is accompanied by a complexity analysis.
- **Extensive experimentation:** We extensively evaluate the

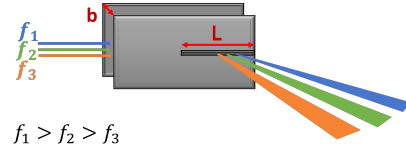


Fig. 1: Beamforming of different frequency components using an LWA with plate separation b and slit length L .

potential of LWAs in facilitating cost-efficient and sustainable THz wireless communications. Our numerical studies reveal that a properly tuned LWA can achieve multiple directed beams and approach the rates supported by costly conventional fully digital MIMO transmitters. We also show that transiting from uniform to non-uniform bandwidth division indeed facilitates exploiting the spectral characteristics of LWA signaling, yielding improved achievable rates and beampatterns, compared to non-optimized even spectral division.

The remainder of this paper is organized as follows: Section II presents the proposed LWA communication model. Joint tuning of the LWA and power allocation is presented and evaluated in Sections III and IV, respectively. Finally, Section V concludes the paper.

II. SYSTEM MODEL AND PROBLEM FORMULATION

In this section, we describe the system model underlying our study. We begin by detailing the characteristics and operational principles of LWAs in Subsection II-A. Then, we present the resulting LWA-aided THz communication system in Subsection II-B, based on which we formulate the problem of optimizing the LWA parameters for enhanced downlink communications in Subsection II-C.

A. LWA Modeling

In its most general form, an LWA consists of two parallel metal plates (though it can also be fabricated using typical complementary metal-oxide semiconductor (CMOS) technology [44]). The plates are separated by a distance denoted by b , and one of the plates has a slit of length L , as illustrated in Fig. 1. As a wideband THz signal travels between the plates, it emerges from the slit at various angles of departure (AoDs) [36]. The emission angle changes monotonically for different frequency components, creating a *THz rainbow* effect at the LWA output. The propagation profile of the signal along the L -length slit radiates spectral components in directed beams in a manner that bears some similarity to synthetic apertures generated by moving devices [45]. To formulate this mathematically, a spectral component at frequency f is radiated at azimuthal angle ϕ_f , as follows [36]:

$$\phi_f = \sin^{-1} \left(\frac{c}{2bf} \right), \quad (1)$$

where c is the speed of light. Since ϕ_f is inversely proportional to f , it can be easily concluded that *higher* frequencies are emitted at *smaller* angles relative to the plate’s axis.

The angular width of each directed monochromatic beam around its maximum emission angle depends on the LWA

parameters L and b , and increases as the frequency f increases. Specifically, the diffraction pattern at angle ϕ and frequency f can be modeled as [36]:

$$G(\phi, f; b, L) = \text{sinc} \left[(\beta - j\alpha - k_0 \cos \phi) \frac{L}{2} \right], \quad (2a)$$

$$\beta \triangleq k_0 \sqrt{1 - \left(\frac{c}{2bf}\right)^2}. \quad (2b)$$

In (2), $k_0 \triangleq \frac{2\pi f}{c}$ is the free-space wave number, and α is a parameter describing the energy loss of the transmitted wave as a result of leakage out of the LWA's slit. This loss is typically negligible, i.e., $\alpha \ll \beta$ [36], and thus, in the following we use $\alpha = 0$.

It follows from the diffraction pattern in (2) that a single LWA can steer THz beams by tuning its L and b physical parameters. Moreover, signal components at different frequencies are radiated at different angles and with different-width beampatterns. This indicates that by optimizing the tuning of the LWA parameters as well as the spectral allocation of the transmitted signal, this antenna structure can efficiently support high-frequency communications. In particular, as we will study in the sequel, LWAs are capable of handling multi-user communication scenarios with diverse beam patterns and high data rates, while using significantly less power compared to fully digital MIMO systems.

B. LWA-Aided Downlink Communications

We consider a multi-user downlink setup where a base station (BS), equipped with a single LWA, wishes to serve K single-antenna users. We study only azimuthal steering in our LWA modeling, assuming all users are located at the same height. We focus on line-of-sight (LOS) settings, which is the expected operating regime of THz systems [46], where each k th user ($k = 1, \dots, K$) is located at a relative distance ρ_k and angle φ_k from the BS. The BS employs wideband signaling with N non-overlapping subbands with central frequencies f_1, \dots, f_N . The signal modulated at each n th subband ($n = 1, \dots, N$) is represented by $x_n \in \mathbb{C}$ (in practice chosen from a discrete modulation set), and its power is denoted by $P_n \geq 0$. In addition, the BS is subject to a total power constraint P , such that it holds that:

$$\sum_{n=1}^N P_n \leq P. \quad (3)$$

The use of an LWA implies that the spectral component at each frequency f_n is emitted at an angle ϕ_{f_n} , as depicted in Fig. 2. The LWA induces a channel whose coherence bandwidth changes inherently with frequency/angle in a manner where higher frequencies or low angles are translated into narrower beams, which in turn impact the coherence bandwidth. Therefore, we depart from the conventional OFDM setting and allow for an uneven division of the frequency band. We denote the subband related to frequency f_n by Δf_n and assume that:

$$\sum_{n=1}^N \Delta f_n = BW = f_{\max} - f_{\min}, \quad (4)$$

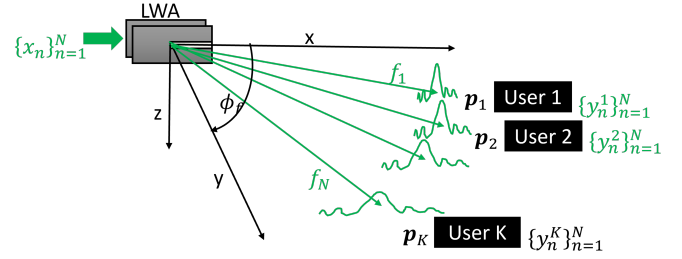


Fig. 2: Downlink THz communications with a single LWA transmitting to K users using N frequency bins.

where BW represents the operational bandwidth, whose lower and upper boundaries are the frequencies f_{\min} and f_{\max} , respectively.

The conventional setting of OFDM signaling is obtained as a special case of the considered communication system model, by restricting all subbands to have equal bandwidth, i.e., $\Delta f_n = \frac{BW}{N}$. For simplicity, we assume that each subband is not larger than its corresponding coherence bandwidth, namely, that Δf_n is sufficiently narrow such that (1) and (2) hold for the entire subband centered at f_n [47, Ch. 2]. To this end, by denoting with d_n the coherence bandwidth around f_n , we impose the following constraint on the subband widths:

$$0 \leq \Delta f_n \leq d_n, \quad \forall n \in \{1, \dots, N\}. \quad (5)$$

Let $y_n^k \in \mathbb{C}$ represent the signal received by each k th user at each n th subband. Accordingly, we introduce the channel input-output relationship, which, based on the LOS assumption, we model as follows:

$$y_n^k = G(\varphi_k, f_n; b, L) \Gamma(\rho_k, f_n) x_n + w_n^k, \quad n = 1, \dots, N, \quad (6)$$

where $\Gamma(\cdot, \cdot)$ is an attenuation coefficient that depends on relative distance ρ_k and the frequency f_n , and w_n^k is spectrally and temporally independent and identically distributed Gaussian noise with variance σ^2 . The function $G(\varphi_k, f_n; b, L)$ is the LWA diffraction pattern at angle φ_k and frequency f_n , defined in (2), and is the key component relating the resulting communications channel (defined in Subsection II-C) to the LWA parameters b, L .

C. LWA Configuration Optimization

Our goal is to leverage the frequency-dependent beam-steering performed by the LWA to support high-rate data transfer in multi-user downlink communication systems. To that aim, we formulate the LWA-based communication channel and characterize the relationship between the achievable rate and the transmitter's controllable parameters. Specifically, the configuration of the LWA, i.e., its physical parameters b and L , affects the channel input-output relationship via the $G(\cdot, \cdot)$ function in (6). Accordingly, in this paper, we focus on tuning b and L along with the power allocation $\{P_n\}_{n=1}^N$ and the subband widths $\{\Delta f_n\}_{n=1}^N$ based on the sum-rate objective.

To formulate the achievable sum-rate performance for a given LWA configuration, we define each n th subband channel vector, $\mathbf{h}_n \in \mathbb{C}^K$, such that:

$$\mathbf{h}_n(b, L, \{\Delta f_n\}_{n=1}^N) = \begin{bmatrix} G(\varphi_1, f_n; b, L)\Gamma(\rho_1, f_n) \\ G(\varphi_2, f_n; b, L)\Gamma(\rho_2, f_n) \\ \vdots \\ G(\varphi_K, f_n; b, L)\Gamma(\rho_K, f_n) \end{bmatrix}. \quad (7)$$

Recall that the subbands $\{\Delta f_n\}_{n=1}^N$ dictate the carrier frequencies via $f_n = f_{\min} + \sum_{j=1}^{n-1} \Delta f_j + \frac{\Delta f_n}{2}$. Moreover, the LWA parameters L and b are typically constrained within some physical ranges, namely $b \in [b_{\min}, b_{\max}]$ and $L \in [L_{\min}, L_{\max}]$, to ensure a certain level of antenna efficiency. Using the notation of (7), the achievable sum-rate performance at each frequency bin f_n is given by the expression [48]:

$$R_n(b, L, P_n, \Delta f_n) = \log \left(1 + \frac{P_n}{\sigma^2} \|\mathbf{h}_n(b, L, \Delta f_n)\|^2 \right). \quad (8)$$

Accordingly, the average achievable sum rate of the wideband transmission is given by:

$$R(b, L, \{P_n\}_{n=1}^N, \{\Delta f_n\}_{n=1}^N) = \sum_{n=1}^N \Delta f_n \log \left(1 + \frac{P_n}{\sigma^2} \|\mathbf{h}_n(b, L, \Delta f_n)\|^2 \right). \quad (9)$$

The common approach for wideband signaling in wireless communications employs OFDM. In this multiplexing scheme, the subbands are equally spaced, and thus, $\Delta f_n = \frac{BW}{N} \forall n \in \{1, \dots, N\}$. When employing LWAs in THz, the width of the lobes of the diffraction pattern in (2) vary considerably with the frequency (and with angle), as illustrated in Fig. 2. This indicates that in LWA-aided THz systems, it is expected to be beneficial to deviate from conventional OFDM, and allow the subbands to vary in their width.

In this work, we aim to maximize the achievable sum-rate performance under given physical and power constraints. Based on the discussion above, the resulting problem of jointly tuning the LWA, the subbands' widths, and the wideband power allocation can be mathematically expressed as follows:

$$\max_{b, L, \{P_n\}_{n=1}^N, \{\Delta f_n\}_{n=1}^N} R(b, L, \{P_n\}_{n=1}^N, \{\Delta f_n\}_{n=1}^N) \quad (10a)$$

$$\text{s.t.} \quad \sum_{n=1}^N P_n \leq P, \quad (10b)$$

$$P_n \geq 0, \quad \forall n \in \{1, \dots, N\}, \quad (10c)$$

$$\sum_{n=1}^N \Delta f_n = BW, \quad (10d)$$

$$0 \leq \Delta f_n \leq d_n, \quad \forall n \in \{1, \dots, N\}, \quad (10e)$$

$$f_n = f_{\min} + \sum_{j=1}^{n-1} \Delta f_j + \frac{\Delta f_n}{2} \quad (10f)$$

$$b_{\min} \leq b \leq b_{\max}, \quad (10g)$$

$$L_{\min} \leq L \leq L_{\max}. \quad (10h)$$

It can be seen that (10) is a non-convex problem due to the complex dependence of the LWA-induced channel on the

optimization parameters, namely, the relationship induced by (2) and (7) between the sum rate, the LWA parameters b and L , and the frequencies $\{f_n\}_{n=1}^N$ determined by the subband division $\{\Delta f_n\}_{n=1}^N$. The first two constraints (10b) and (10c) ensure that the power allocation withholds the total power constraint P , and that the optimized powers are non-negative values, as physically dictated. Next, constraints (10d)–(10f) govern the division of the frequency band, ensuring that the optimized carrier frequencies are monotonically non-decreasing, while supporting non-overlapping subbands that sum up to the entire available bandwidth. In addition, constraint (10e) ensures that the allocated subbands withhold a physically compliant coherence width. Similarly, the constraints (10g) and (10h) over b and L , respectively, ensure that the scales of the LWA parameters satisfy the physical assumptions necessary for formulating the expressions in (1) and (2).

III. LWA-AIDED DOWNLINK BEAMFORMING

In this section, we develop an alternating optimization framework for LWA-aided downlink beamforming in multi-user THz communication systems, based on our characterization of the channel model and the resulting sum-rate performance included in the previous Section II. We note that our design optimization problem (10) is non-convex due to the complex dependence on b , L , and $\{\Delta f_n\}_{n=1}^N$. However, when treating each set of optimization variables separately, the problems become simpler. Hence, we adopt an alternating optimization approach to set the tunable parameters based on the considered sum-rate objective. Specifically, we first focus on optimizing the LWA configuration parameters, i.e., b and L , as described in Subsection III-A. Then, we discuss the setting of the power allocation $\{P_n\}_{n=1}^N$ in Subsection III-B, and how it is combined into the joint setting of the subband power and width, $\{P_n\}_{n=1}^N$ and $\{\Delta f_n\}_{n=1}^N$, in Subsection III-C. The overall algorithm is summarized in Subsection III-D, and its properties are discussed in Subsection III-E.

A. LWA Configuration

We start by optimizing the LWA configuration b and L for fixed values of $\{P_n\}_{n=1}^N$ and $\{\Delta f_n\}_{n=1}^N$. We focus on the i th iteration of the overall alternating optimization, and thus, set the subband configuration parameters to be those obtained from the previous iteration, denoting them by $\{P_n^{(i-1)}, \Delta f_n^{(i-1)}\}_{n=1}^N$.

Since the sum-rate objective is a non-convex function of b and L , and both optimization decision variables are scalars taking value in some bounded range, we tune b and L for fixed $\{P_n\}_{n=1}^N$ and $\{f_n\}_{n=1}^N$ using a grid search. Specifically, we divide the ranges $[b_{\min}, b_{\max}]$ and $[L_{\min}, L_{\max}]$ into uniformly spaced grids, denoted by $\mathcal{B}_{\text{grid}}$ and $\mathcal{L}_{\text{grid}}$, respectively, such that the constraints in (10g) and (10h) are satisfied. By substituting these values in the optimization problem (10), all the constraints are redundant. Thus, we obtain that, at each i th iteration, one should scan all possible combinations on the grid to set as follows:

$$(b^{(i)}, L^{(i)}) = \arg \max_{b, L \in \mathcal{B}_{\text{grid}} \times \mathcal{L}_{\text{grid}}} R \left(b, L, \{P_n^{(i-1)}\}_{n=1}^N, \{\Delta f_n^{(i-1)}\}_{n=1}^N \right). \quad (11)$$

It can be seen that the complexity of solving (11) depends on the grid resolution, as it involves $|\mathcal{B}_{\text{grid}}||\mathcal{L}_{\text{grid}}|$ ($|\cdot|$ returns the set cardinality) evaluations of the sum-rate objective.

B. Spectral Power Allocation

We proceed to the optimization of the power allocation $\{P_n\}_{n=1}^N$. It can be seen from (9) that the sum-rate objective is a convex function of $\{P_n\}_{n=1}^N$, when b , L , and $\{\Delta f_n\}_{n=1}^N$ are fixed. Accordingly, we focus on the i th iteration of the overall alternating optimization algorithm, where the remaining optimization variables b , L , and $\{\Delta f_n\}_{n=1}^N$ are set to $b^{(i)}$, $L^{(i)}$, and $\{\Delta f_n^{(i)}\}_{n=1}^N$, respectively. By substituting these values into the optimization problem in (10), we obtain that at each i th iteration, we need to set:

$$\begin{aligned} \{P_n^{(i)}\} &= \arg \max_{\{P_n\}_{n=1}^N} R(b^{(i)}, L^{(i)}, \{P_n\}, \{\Delta f_n^{(i)}\}) \\ \text{s.t.} \quad &\sum_{n=1}^N P_n \leq P, \\ &P_n \geq 0, \quad \forall n \in \{1, \dots, N\}. \end{aligned} \quad (12)$$

It can be easily concluded via (9) and the convexity of its constraints that (12) is a convex optimization problem. We note that the conventional OFDM setting is a special case of (12), which is obtained for equal power allocation, i.e., $\Delta f_n = \frac{BW}{N}$, and is known to be solved via waterfilling [47, Ch. 5.3]. While in our formulation we allow non-identical subbands to exploit the diverse spectral profile of LWAs, the resulting optimal power allocation is obtained as an extension of the classical waterfilling solution, as stated in the following lemma.

Lemma 1: The optimal power allocation in (12) is given by

$$P_n^{(i)} = \max \left\{ \frac{\Delta f_n^{(i)}}{\nu} - \frac{\sigma}{\|\mathbf{h}_n(b^{(i)}, L^{(i)}, \{\Delta f_l^{(i)}\}_{l=1}^N)\|^2}, 0 \right\}, \quad (13)$$

where $\nu > 0$ is set such that $\sum_{n=1}^N P_n^{(i)} = P$.

Proof: The lemma is obtained from [49, Sec. II-C]. ■

The power allocation in (13) is given in closed form. However, finding the exact setting of ν usually involves searching methods, with typical worst-case complexity order of $\mathcal{O}(N^2)$ [49], [50].

C. Subband Configuration

Now, we set b and L to $b^{(i)}$ and $L^{(i)}$, respectively, as optimized in Subsection III-A and optimize the subband division. We recall the strong coupling between the power allocation and the subband division, and thus, leverage the result in Subsection III-B to optimize the power allocation within the review of each considered subband division. First, to optimize the subband division $\{\Delta f_n\}_{n=1}^N$ given $b^{(i)}$ and $L^{(i)}$, we propose a recursive grid search method we name *Greedy Grid Search*. As the name suggests, at the i th iteration, we operate in a greedy manner by updating the parameters sequentially: first $\Delta f_1^{(i)}$, then $\Delta f_2^{(i)}$, followed by $\Delta f_3^{(i)}$, and so on. The tuning of each $\Delta f_n^{(i)}$ is done by searching over

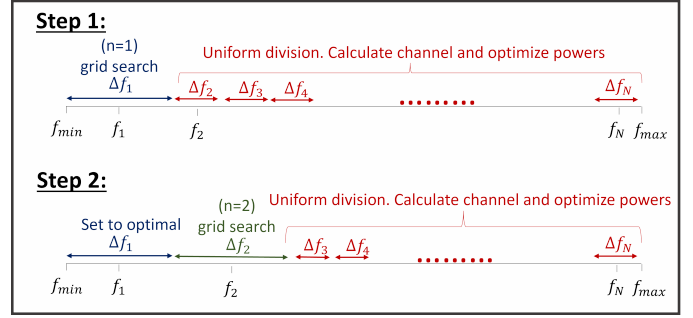


Fig. 3: Optimization of the first two frequency widths $\Delta f_1^{(i)}$ and $\Delta f_2^{(i)}$ using the proposed *Greedy Grid Search* summarized in Algorithm 1.

a grid denoted by $\mathcal{F}_{n,\text{grid}}^{(i)}$. When inspecting each point in the grid, the subsequent (not yet set) subbands are set by uniform division of the remaining bandwidth. An illustration of this operation is depicted in Fig. 3.

We sequentially adjust each subband width $\Delta f_n^{(i)}$ by performing a grid search over its possible values. We fix the previous subbands to the optimized widths found in previous iterations i.e., $\{\Delta f_j^{(i)}\}_{j=1}^{n-1}$, and divide the range of possible $\Delta f_n^{(i)}$ into the uniformly spaced grid $\mathcal{F}_{n,\text{grid}}^{(i)}$. The grid should be set with maximum and minimum values guaranteeing that the remaining frequencies can be uniformly placed with widths not surpassing the coherence bandwidth constraint in (4).

When scanning a grid point $\Delta f_n \in \mathcal{F}_{n,\text{grid}}^{(i)}$, the subbands $\{\Delta f_j\}_{j=n+1}^N$ are set by an equal division of the remaining bandwidth, namely, for each $j \in \{n+1, \dots, N\}$, we set:

$$\Delta f_j = \frac{BW - \sum_{l=j}^{n-1} \Delta f_l^{(i)} - \Delta f_n}{N - n}. \quad (14)$$

For the resulting subband division, the rate is evaluated using (9), with power allocations set using Lemma 1. Accordingly, we set each n th subband width at each i th iteration of the overall alternating optimization via the following solution:

$$\begin{aligned} \Delta f_n^{(i)} &= \arg \max_{\Delta f_n \in \mathcal{F}_{n,\text{grid}}^{(i)}} R(b^{(i)}, L^{(i)}, \{P_l\}, \\ &\quad \{\Delta f_1^{(i)}, \dots, \Delta f_{n-1}^{(i)}, \Delta f_n, \Delta f_{n+1}, \dots, \Delta f_N\}), \quad (15) \\ \text{s.t.} \quad &\left\{ \begin{array}{l} \Delta f_j \text{ from (14)}, \quad \forall j \in \{n+1, \dots, N\}, \\ \{P_l\}_{l=1}^N \text{ from Lemma 1.} \end{array} \right. \end{aligned}$$

The complexity of solving (15) depends on the size of the grid. Specifically, for each of the N subbands, Algorithm 1 scans a grid of $|\mathcal{F}_{n,\text{grid}}^{(i)}|$ candidates, and computes Lemma 1 for each. Assuming all grids have the same cardinality, such that one can write $|\mathcal{F}_{n,\text{grid}}^{(i)}| = |\mathcal{F}_{\text{grid}}|$, then Algorithm 1 involves $N|\mathcal{F}_{\text{grid}}|$ evaluations of the achievable sum-rate performance, each including computation of Lemma 1 (at a worst-case complexity order of $\mathcal{O}(N^2)$).

We embed in this setting the tuning of the power allocation, detailed in the previous subsection. The resulting procedure is summarized as Algorithm 1.

Algorithm 1: Greedy Grid Search

Input: Users positions $\{\varphi_k, \rho_k\}_{k=1}^K$; power P ;
 LWA configuration $b^{(i)}$ and $L^{(i)}$;
 bandwidth $[f_{min}, f_{max}]$.

- 1 **for** $n = 1, \dots, N$ **do**
- 2 Set search grid $\mathcal{F}_{n, \text{grid}}^{(i)}$ such that (4) and (5) hold;
- 3 **for** $\Delta f_n \in \mathcal{F}_{n, \text{grid}}^{(i)}$ **do**
- 4 Divide the remaining bandwidth via (14) ;
- 5 Compute power allocation using (13);
- 6 Grid search for $\Delta f_n^{(i)}$ via (15) ;
- 7 Compute $\{P_n^{(i)}\}_{n=1}^N$ for $\{\Delta f_n^{(i)}\}_{n=1}^N$ using Lemma 1;
- 8 **return** $\{\Delta f_n^{(i)}\}_{n=1}^N, \{P_n^{(i)}\}_{n=1}^N$.

D. Overall Algorithm Solving (10)

The individual tools for setting each of the optimization variables dictating the beampattern achieved with the proposed LWA-aided downlink communications are combined into an overall beamforming algorithm based on alternating optimization. We identify differences in the basic characteristics of the problems' parameters that can be divided into two groups: *i)* b and L are the physical scales of the LWA, hence, both share similar constraints in (10); *ii)* The constraints on $\{\Delta f_n\}_{n=1}^N$ are more complex and strongly affect the optimization of $\{P_n\}_{n=1}^N$, which depend on the carrier frequency setting determined by the subband widths. Consequently, our proposed algorithm alternates between two main steps: *i)* Optimizing the LWA configuration b and L for fixed $\{P_n\}_{n=1}^N$ and $\{\Delta f_n\}_{n=1}^N$ (as detailed in Subsection III-A); and *ii)* setting the subband division $\{\Delta f_n\}_{n=1}^N$ and the power allocation $\{P_n\}_{n=1}^N$ for fixed LWA b and L (based on the Greedy Grid Search developed in Subsection III-C). The overall procedure for solving (10) is summarized in Algorithm 2.

Algorithm 2: LWA Beamforming Optimization

Initialization: Set $P_n^{(0)} = \frac{P}{N}$ and the maximum iterations to i_{\max} .

Input : Users positions $\{\varphi_k, \rho_k\}_{k=1}^K$; total power P ; bandwidth $[f_{min}, f_{max}]$.

- 1 **for** $i = 1, \dots, i_{\max}$ **do**
- 2 Grid search for $(b^{(i)}, L^{(i)})$ via (11);
- 3 Set $\{\Delta f_n^{(i)}\}_{n=1}^N$ and $\{P_n^{(i)}\}_{n=1}^N$ using Algorithm 1;
- 4 **return** $b^{(i_{\max})}, L^{(i_{\max})}, \{\Delta f_n^{(i_{\max})}\}_{n=1}^N, \{P_n^{(i_{\max})}\}_{n=1}^N$.

Complexity: We note that Algorithm 2 iterates i_{\max} times between grid searching over (11) and applying Algorithm 1. As noted in Subsection III-A, the former involves complexity order of $\mathcal{O}(|\mathcal{B}_{\text{grid}}||\mathcal{L}_{\text{grid}}|)$. The application of Algorithm 1 involves computing (13) a total of $(N-1)|\mathcal{F}_{\text{grid}}|$ times, whose (worst-case) complexity order is $\mathcal{O}(N^3|\mathcal{F}_{\text{grid}}|)$. Accordingly, the overall complexity of Algorithm 2 is of the order

$$\mathcal{O}(i_{\max} (|\mathcal{B}_{\text{grid}}||\mathcal{L}_{\text{grid}}| + N^3|\mathcal{F}_{\text{grid}}|)). \quad (16)$$

The complexity order in (16) consists of two summands, representing the two main stages of Algorithm 2. The identity of the dominant term depends on the grid sizes.

E. Discussion

Our proposed physically compliant modeling of LWA-based wireless communications facilitates unveiling the potential of this antenna technology for future high-frequency wireless systems. From a hardware perspective, the LWA technology has notable gains in terms of cost and power consumption due to its ability to steer wideband THz beams in a controllable manner with a single element. This approach eliminates the need for numerous wideband radio frequency chains and analog beamformers, which becomes extremely costly at THz frequencies and are typically employed by conventional massive MIMO architectures.

The proposed alternating optimization method in Algorithm 2 for solving (10) provides a means to tune LWAs to achieve desirable beampatterns that support multiple users. This capability is numerically demonstrated in the following Section IV. We note that the computational burden of tuning the LWA via Algorithm 2 is dictated by the grid sizes, the number of iterations, and the complexity of the extended waterfilling approach. The former two factors are design hyperparameters, which can be configured based on a desired complexity level. Computing (13) involves an iterative search, whose complexity grows quadratically with N in the worst case, and often grows only linearly with N (depending on how many subchannels are active) [49].

In our proposed Algorithm 2, we opted not to include the optimization of the power allocation using waterfilling during the tuning of the LWA physical parameters b and L . Similar to the optimization of the spectral division, tuning the LWA impacts the channel representation based on which the power allocation was optimized. However, we perceive the coupling between the LWA parameters and the optimal power allocation to be somewhat weaker than the coupling between the spectral division and the power allocation, while the grid sizes we choose for the search of b and L are notably larger than the grid size of the spectral width of each subband, and of the number of frequencies N . Therefore, we choose to alleviate the additional computational complexity and leave the impact of tuning the power allocation simultaneously with b and L for future investigation.

In our modeling of the communication configuration, we deviate from the conventional OFDM model. In OFDM, the frequency band is evenly divided to monochromatic subchannels, designed to have subbands that do not surpass the worst case coherence duration [47, Ch. 3.4]. Such traditional designs struggle to faithfully capture the coherence bandwidth variability induced by LWAs, motivating to optimize the frequency band division to fit the LWA's particular behavior in the frequency domain. This deviation into non-identical subband widths allows for achieving improved sum-rate performance compared to conventional equal subbands, as we numerically demonstrate in the following Section IV, though it potentially necessitates additional network management.

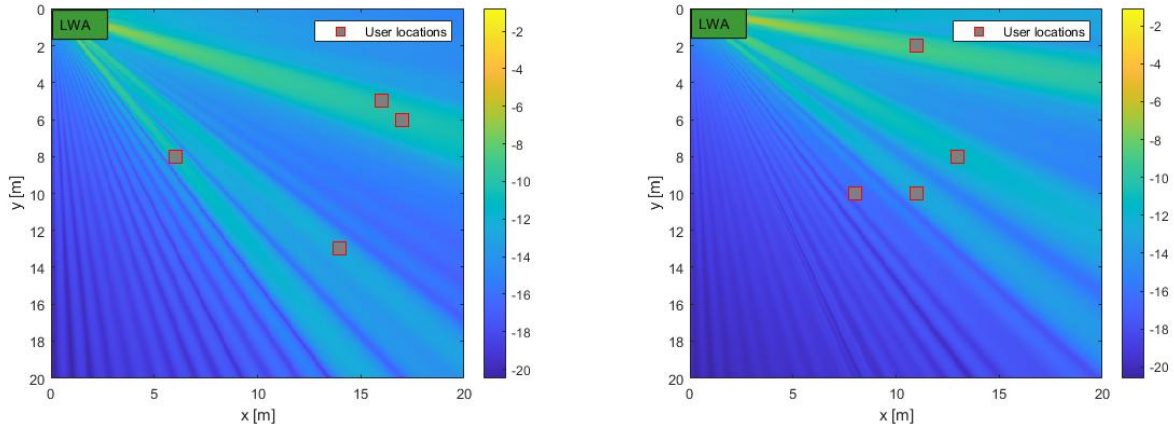
(a) Directed beams towards all $K = 4$ users.(b) Directed beams towards 3 out of $K = 4$ users.

Fig. 4: Beampatterns achieved using a single LWA with bandwidth division optimization. The coordinate system is compliant with Fig. 2.

We finally note that the LWA communication model in (6) is formulated for a generic path loss function $\Gamma(\cdot, \cdot)$. Thus, while we set it to be range-dependent for simplicity, one can also use frequency-dependent profiles, which are expected to be encountered in THz. Moreover, while our beampattern design is based on the sum-rate maximization in (10), alternative relevant problems that follow from the LWA model can be considered. For instance, (10) is formulated assuming that the users can process the full wideband signals, while users may operate at a given subband. In addition, we do not consider any specific access control protocol for user synchronization, and currently focus on the upper bound for the achievable rate calculated by (8). Further, in practice, the LWA configuration parameters b and L are controlled via mechanical measures, which may constrain how frequently they can be modified. Finally, our formulation assumes that the users' locations are known, without exploring how they are recovered by an LWA-aided BS. However, very recently, [51] have shown that employing THz rainbow transmissions can in fact facilitate acquiring such localization estimates, which can be potentially combined with our subsequent beamforming task. These extensions of our study, whose aim is to introduce the framework of LWA-aided communications and its potential for THz systems, are left for future work.

IV. NUMERICAL RESULTS AND DISCUSSION

In this section, we numerically evaluate the ability of LWA-equipped BSs in supporting multiple downlink users via our proposed beamforming design¹. We first illustrate the beampatterns achieved using a single LWA, after which we compare the resulting sum rates to those achievable using (extremely costly) fully digital wideband THz MIMO signaling. In our numerical study, we examine two setups: a small-scale scenario with $K = 4$ users and a larger scenario with $K = 16$ users. Using the small-scale scenario, we evaluate the ability of our single-LWA-based communications channel

to perform beamsteering towards given user locations and support high-rate communications. We demonstrate the gains of deviating from the OFDM setting when working with LWAs by allowing flexibility in the bandwidth division, and compare the achievable rates to those predicted to be achieved by the currently-researched fully digital MIMO setting. Then, we extend our simulations to the larger scenario to validate that the trends we recognize hold for a larger, multi-user setting.

A. LWA Beampatterns

To evaluate the capability of a LWA-aided BS in generating directional beams, we consider the channel model detailed in Section II in the frequency range of $[0.2, 0.8]$ THz divided into $N = 150$ frequency bins, with the subband width constraints of $d_n = d = \frac{BW}{40} \forall n$. We randomize $K = 4$ users with relative angles and distances drawn uniformly in the ranges $[10, 55]^\circ$ and $[10, 20]$ meters, respectively. For each setting, we use the proposed Algorithm 2 to tune the LWA configuration within the ranges $[b_{\min}, b_{\max}] = [0.9, 1.1]$ mm and $[L_{\min}, L_{\max}] = [10, 50]$ mm, along with the power allocation and the bandwidth division, where we use the total power constraint $P = 10\sigma^2$.

In Fig. 4, we illustrate two different beampatterns, i.e., the energy radiated towards each position (φ, ρ) over the entire spectrum. The energy at each position is computed in logscale as $\log(\sum_{n=1}^N |G(\varphi, f_n)\Gamma(\rho, f_n)|^2 P_n)$ using our proposed Algorithm 2, while optimizing the bandwidth division using our proposed Algorithm 1. For simplicity, we have set the attenuation coefficient to scale as $\Gamma(\rho, f) \propto 1/\rho$. It can be observed in Fig. 4 that a single LWA can generate relatively directed beams. Seemingly similar beampatterns can be achieved by the LWA channel under the OFDM setting, as depicted in Fig. 5, though the achieved rates in such case are lower, as we discuss in more detail next in Subsection IV-C.

Observing the beampatterns in Figs. 4 and 5, we recognize the inherent lack of symmetry of the LWA-based channel towards user locations/frequencies. Specifically, as the AoD changes monotonically with the frequency by (1), users located

¹The source code and hyperparameters used in this experimental study is available at: https://github.com/yeelagn/LWA_communications.git.

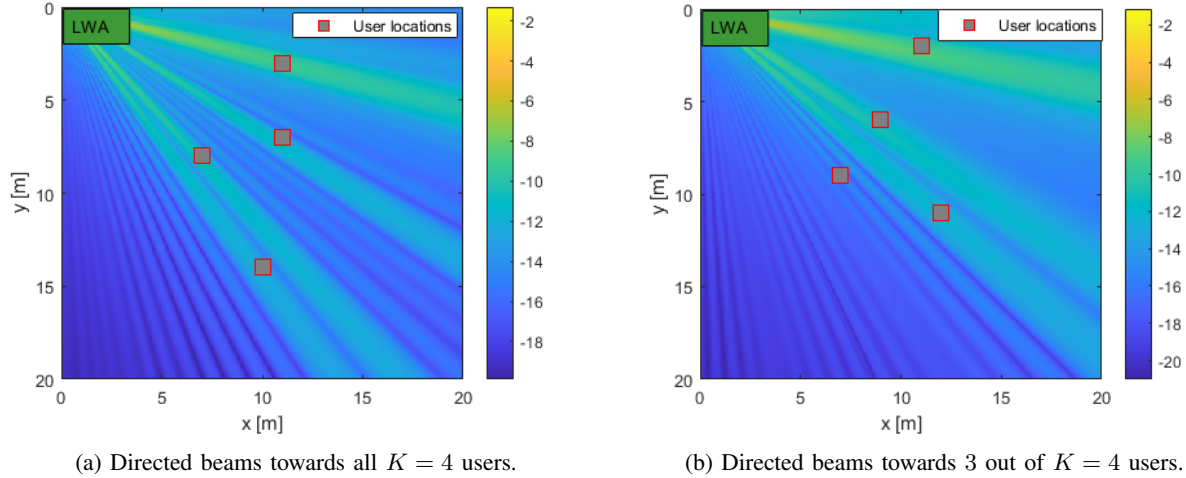


Fig. 5: Beampatterns achieved using a single LWA with OFDM. The coordinate system is compliant with Fig. 2.

at small angles with respect to the LWA axis communicate at higher frequencies (with transmission power spread over multiple bins), unlike those located at larger angles. By inspecting (2), it is also evident that a monochromatic beam's width is dependent on the beam's frequency, as β and k_0 are functions of f , and thus, higher frequency components are steered into narrower and more accurate beams. Consequently, for a system with users of similar distance from the LWA and equal power allocation for all engaging frequency components, the LWA-induced channel can naturally achieve higher rates communicating with users at smaller angles (and higher frequencies). Accordingly, the proposed Algorithm 2 is prone to assign more resources to steering beams towards the users with smaller angles. This can result in a relatively balanced service of multiple users, as in Figs. 4a and 5a, or alternatively, steering most of the signal power towards users at lower angles, as in Figs. 4b and 5b. These beampatterns show the ability of a LWA to generate directed beams, and also indicate that in settings where it is crucial to guarantee balanced service of multiple users, alternative objectives, e.g., minimal rate, should be considered.

B. Bandwidth Division and Power Allocation

The formulation of the achievable sum-rate performance in a manner which is not confined to OFDM builds on the assumption that each subband width does not exceed its corresponding coherence bandwidth d . For this purpose, one has to limit the allocated subbands' widths to ensure that each frequency subband can be well represented by computing (2) and (7), and that the channel behavior is approximately constant for all frequencies under the same subband. To ensure that this assumption does hold, we next visualize the sub-channel norms calculated for various settings, as achieved by the LWA-optimized channel.

For reference, we begin by depicting the obtained power allocation and corresponding channel norms when using OFDM signaling in Fig. 6. The resulting profiles are then compared with the corresponding channel norms induced when optimizing the spectral division for LWA-aided multi-user

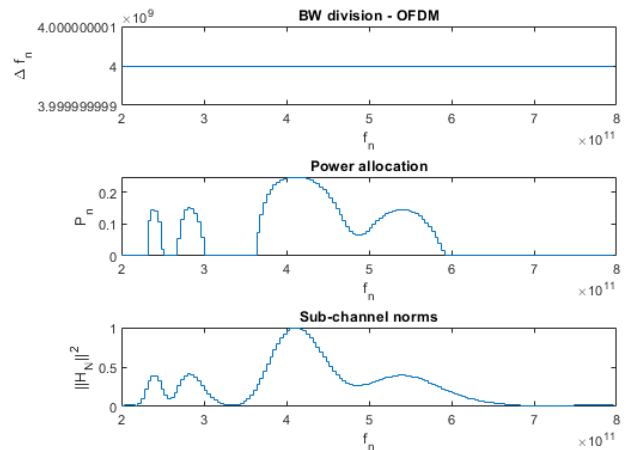
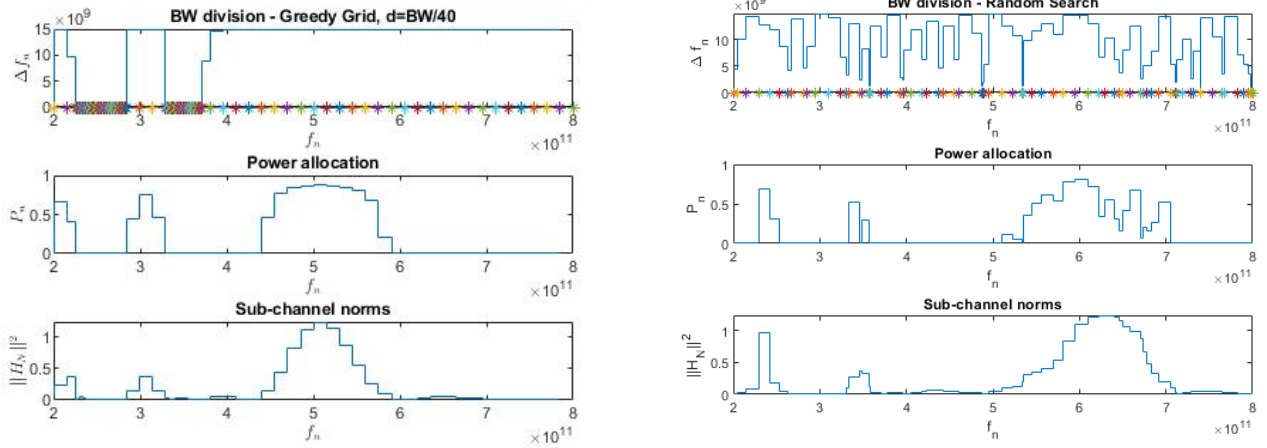


Fig. 6: Bandwidth division and corresponding channel norm for OFDM with narrow subband spacing of $\Delta f_n = \frac{BW}{150}$.

communications in Fig. 7. There, we consider both tuning the spectral division using our proposed Algorithm 1 in Fig. 7a, as well as optimization via random search in Fig. 7b. Observing Fig. 7a and Fig. 7b, we note that in both optimization methods, the resulting plots for the sub-channel norms portray piecewise-constant curves that can be considered as good approximations to the channel representation achieved under the OFDM setting. We, thus, conclude that the choice $d = BW/40$ used in our simulation study is a tight enough constraint over the coherence width. Tighter constraints would naturally, keep the physical demands of the system. However, we advise not to choose an overly loose constraint under the given setting since the results may no longer represent physically achievable sum-rate performance.

In addition to the channel norm plots, we depict in Fig. 7 the bandwidth divisions achieved by the different optimization algorithms, as well as the corresponding power allocations. Our results demonstrate that by enabling a flexible division of the frequency band, the LWA signaling effectively exploits the more favorable frequency bands by allocating minimal width to certain bands, while maximizing the width of sub-



(a) BW divided using the proposed Greedy Grid Algorithm 1, (b) BW divided using Random Search over $\{\Delta f_n\}_{n=1}^N$, considering the subband maximum width constraint $d = BW/40$. the subband maximum width constraint $d = BW/40$.

Fig. 7: Visualizations of the bandwidth division and the corresponding channel norms as well as the power allocation. The borders between subbands are represented by '*' markers. We have chosen $d = BW/40$ to ensure good representation of the channel behavior.

channels corresponding to valuable frequencies with large channel norms. Hence, the dedicated optimization method enables to properly exploit the channel characteristics induced by the considered LWA technology without violating the underlying assumption of approximately flat sub-channels.

C. Achievable Sum-Rate Performance

We proceed to evaluate the achievable sum-rate performance and compare it to that achieved with a fully digital MIMO system. We consider the same wideband setting as in Subsection IV-A, under the small-scale scenario with $K = 4$ users. We have optimized the sum rate and compare the results for three optimization approaches: *i*) an LWA with traditional non-optimized OFDM, i.e., even division of the bandwidth (with only the LWA parameters and the power allocation optimized); *ii*) an LWA optimized via the proposed Algorithm 2 with the proposed Greedy Grid solution for the bandwidth optimization (Algorithm 1); and *iii*) an LWA whose spectral division is obtained by a random search over possible bandwidth divisions. For each LWA approach, we have computed the sum rate in bits-per-second, averaged over 30 different randomized locations of the users. In addition, we compare the LWA with a fully digital wideband multi-antenna BS equipped with a uniform linear array with M half-wavelength spaced elements centered at the origin, corresponding to the antenna position in the LWA-based channel. The sum-rate curves in the figure have been computed using spatial-spectral waterfilling [52].

Since the channel model is tightly related to the antenna architecture, for the MIMO setting, we obtain the channel using the LOS model of [53] encompassing both radiative near- and far-field users. To guarantee a fair comparison, we normalize the MIMO channels to have the same max tap magnitude as the LWA channel, and compute the sum rate versus the average SNR, defined as $\text{SNR} = \frac{P}{N\sigma^2}$. We only normalize the MIMO channels to ensure that the optimization

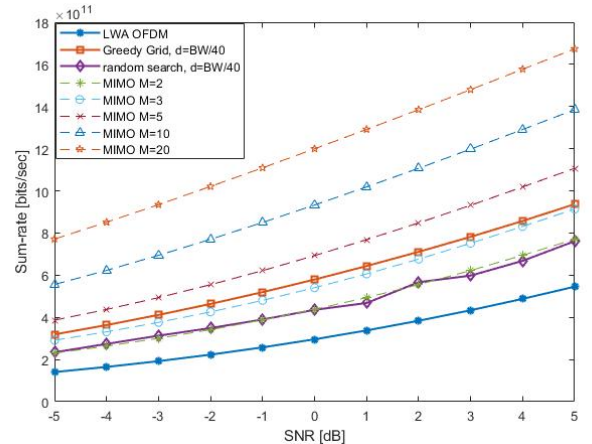


Fig. 8: Sum-rate performance versus the signal-to-noise ratio (SNR) for $K = 4$ users, comparing LWA-based approaches and fully digital MIMO with M transmit antennas.

algorithm suggested in Subsection III-D offers a solution independent of the channel normalization.

Although our study in Subsection IV-B indicates that our design does not lead to a setting that violates the assumption of approximately flat sub-channels, we ensure that the rates we report hold, regardless of the maximal coherence width d we choose. Specifically, we adjust the rate calculation to be based on the optimized power allocation of each individual algorithm, while resampling the proposed power allocation and the corresponding frequencies in the same thinly-divided frequency choice of the OFDM setting, i.e., $f_n = f_{\min} + \frac{BW}{N_f} n \forall n$. Calculating the sum rate this way assures that the resulting curves reported indeed hold (in the same sense as the computation of the OFDM rate is) regardless of the maximal spectral width constraint that is imposed.

The results reported in Fig. 8 show that the sum rate

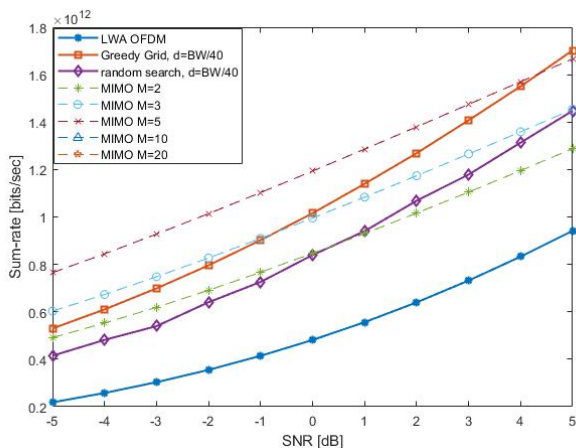
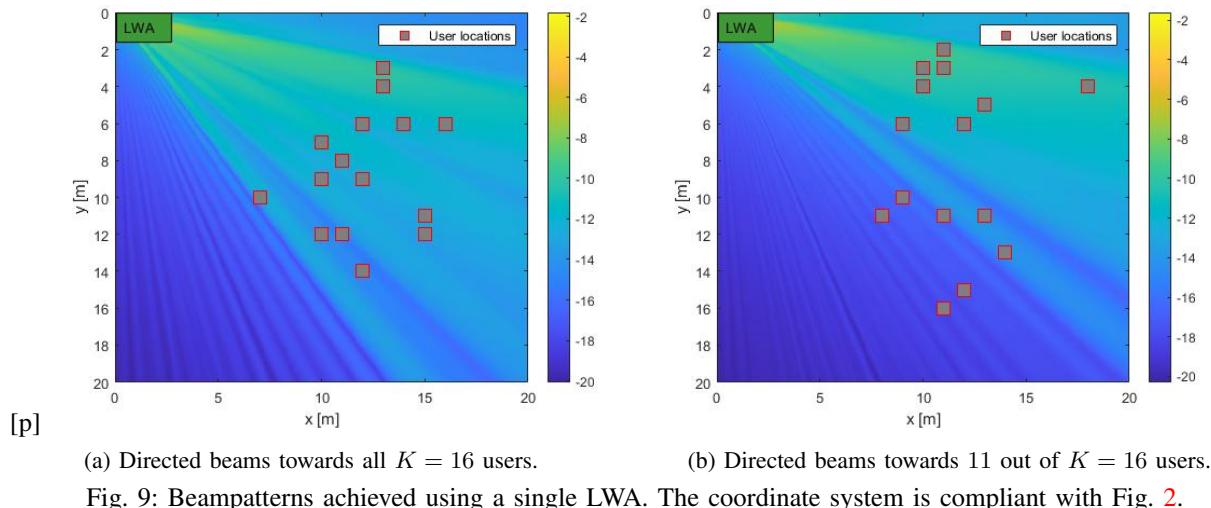


Fig. 10: Sum-rate performance versus the SNR for $K = 16$ users, comparing LWA-based approaches and fully digital MIMO with M transmit antennas.

achieved by a LWA-based channel is comparable to the sum-rates achieved by the MIMO setting, and may offer a valuable alternative to the (costly and currently non-feasible at THz) traditional setting, while supporting wideband transmissions. We note that in the MIMO setting, the beamforming is induced by manipulating the interference of correlated signals transmitted from multiple antennas, and thus the increase of the number of antennas, M , enables the forming of better directed beams and therefore increase the achievable rate. As a trade-off, the increase of M is accompanied by an increase in the number of costly phase shifters which also consume additional power. Comparing the rates achieved by the LWA under the OFDM setting vs. the results acquired when optimizing the bandwidth division, it is evident that the added flexibility of optimizing the frequency band division in a non-uniform way highly improves the achievable rates results. We also note that, as the problem suggested in (10) is highly non-convex and complex, the offered solution from the Greedy Grid Algorithm 1 is not optimal, and further investigation of solutions may increase the achievable sum rate substantially. As evidence, we see that solving the exact same optimization

problem using a random search for $\{\Delta f_n\}_{n=1}^N$, instead of the Greedy Grid, reduces the rates for all SNR values, thus, we deduce that the choice of optimization solution can notably affect the resulting rates achieved in LWA-aided multi-user THz communications.

D. Large-Scale Multi-User Scenario

We now expand our simulations to a large-scale scenario of $K = 16$ users. The remaining setup parameters are chosen to be the same as in Subsection IV-A. Similar to the small-scale scenario, we first visualize candidate beam patterns achieved in Fig. 9. By observing this figure, we note that the LWA-based channel, set according to our proposed Algorithm 2, manages to form relatively directed beams towards given user locations. Once again, we witness that some settings are matched with a solution that steers beams towards all $K = 16$ user locations, as demonstrated in Fig. 9a, while in other cases the beams are steered only towards a partial group of users, with notable preference towards users located at small angles, as demonstrated in Fig. 9b. These results also demonstrate the benefits of leveraging the dispersed angular range, facilitated by the THz rainbow that is created by LWAs, in supporting a large number of users using a single transmit antenna element.

We have also repeated the sum-rate comparison depicted in Subsection IV-C for the large-scale scenario of $K = 16$ users. The results depicted in Fig. 10 show that the trends in terms of performance, compared to costly MIMO antennas noted for few users, hold when the number of users grows. Once again, we see that the LWA-based channel supports communication rates that are comparable to the ones predicted under the fully digital MIMO setting, and that the sum rate significantly raises when optimizing the subband division. The optimized configurations set by our proposed Algorithm 2 achieves rates that are approximately doubled when optimizing the subband division using the Greedy Grid in Algorithm 1, as compared to the LWA-induced channel optimized only with respect to the LWA parameters b and L and the power allocation, with an evenly-divided frequency band (following the traditional OFDM formulation).

Unlike the small-scale case, in the large-scale scenario, the LWA-based channel demonstrates a different response to changes of the SNR than the MIMO channel. The results associated with the LWA show a faster increase in sum rate when increasing the SNR. We conjecture that the change in response to SNR is related to the change in user sparsity with respect to the beams' widths. When the users are sparse, often each user is allocated different frequencies, corresponding to different beams. However, as the number of users grows, more users fall into the angle range covered by a single frequency beam, and this may increase or decrease the effect of the SNR-based power allocation on the resulting rates.

V. CONCLUSIONS

In this paper, we studied wideband downlink multi-user communications at THz frequencies using the LWA antenna technology. We introduced a model for LWA-aided communications that faithfully captures its physical operations, while encapsulating the ability of LWAs to generate frequency-selective directed THz beams with a single antenna element. We proposed an alternating optimization method for jointly tuning the LWA configuration alongside the spectral power allocation. In addition, we suggested that, due to the non-symmetrical nature of the LWA with respect to frequency, an optimizable non-even division of the frequency band may be beneficial in increasing the performance of the LWA-induced wireless channel. Our extensive numerical results showcased that a single LWA can generate directed beams towards multiple users, and achieve sum-rate performance comparable to a (extremely costly) fully digital MIMO array. The achievable sum rates improved significantly when deviating from the conventional OFDM setting and optimizing the frequency band division. These results held for a small-scale scenario of $K = 4$ users, as well as a large-scale one with $K = 16$ users.

The concept of leveraging the THz rainbow induced by LWAs to perform downlink communications with multiple users has only recently emerged, and have not yet been studied extensively. In this paper, we focused on unveiling the potential of this approach in performing high rate communications, compared to traditional MIMO, and analyzed the achievable rate under an ideal scenario of users that are non-selective towards frequency, which can communicate simultaneously and are set at given locations. Our promising results set the ground for extensive future research, e.g., in formatting the paradigm for user localization, access control protocol, rate optimization for frequency-selective users, etc.

REFERENCES

- [1] Y. Gabay, N. Shlezinger, T. Routtenberg, Y. Ghasempour, G. C. Alexandropoulos, and Y. C. Eldar, "Leaky waveguide antennas for downlink wideband THz communications," in *IEEE International Conference on Acoustics, Speech, and Signal Processing (ICASSP)*, 2024, pp. 9111–9115.
- [2] M. Giordani, M. Polese, M. Mezzavilla, S. Rangan, and M. Zorzi, "Toward 6G networks: Use cases and technologies," *IEEE Commun. Mag.*, vol. 58, no. 3, pp. 55–61, 2020.
- [3] C.-X. Wang, J. Wang, S. Hu, Z. H. Jiang, J. Tao, and F. Yan, "Key technologies in 6G terahertz wireless communication systems: A survey," *IEEE Veh. Technol. Mag.*, vol. 16, no. 4, pp. 27–37, 2021.
- [4] W. Jiang, Q. Zhou, J. He, M. A. Habibi, S. Melnyk, M. El-Absi, B. Han, M. Di Renzo, H. D. Schotten, F.-L. Luo, T. S. El-Bawab, M. Juntti, M. Debbah, and V. C. M. Leung, "Terahertz communications and sensing for 6G and beyond: A comprehensive review," *IEEE Commun. Surveys Tuts.*, 2024.
- [5] W. Saad, M. Bennis, and M. Chen, "A vision of 6G wireless systems: Applications, trends, technologies, and open research problems," *IEEE Netw.*, vol. 34, no. 3, pp. 134–142, 2019.
- [6] T. S. Rappaport, Y. Xing, O. Kanhere, S. Ju, A. Madanayake, S. Mandal, A. Alkhateeb, and G. C. Trichopoulos, "Wireless communications and applications above 100 GHz: Opportunities and challenges for 6G and beyond," *IEEE Access*, vol. 7, pp. 78 729–78 757, 2019.
- [7] N. Rajatheva *et al.*, "White paper on broadband connectivity in 6G," *arXiv preprint arXiv:2004.14247*, 2020.
- [8] M. Polese, J. M. Jornet, T. Melodia, and M. Zorzi, "Toward end-to-end, full-stack 6G terahertz networks," *IEEE Commun. Mag.*, vol. 58, no. 11, pp. 48–54, 2020.
- [9] I. F. Akyildiz, C. Han, Z. Hu, S. Nie, and J. M. Jornet, "Terahertz band communication: An old problem revisited and research directions for the next decade," *IEEE Trans. Commun.*, vol. 70, no. 6, pp. 4250–4285, 2022.
- [10] N. T. Nguyen, M. Ma, O. Lavi, N. Shlezinger, Y. C. Eldar, A. L. Swindlehurst, and M. Juntti, "Deep unfolding hybrid beamforming designs for thz massive mimo systems," *IEEE Transactions on Signal Processing*, 2023.
- [11] I. E. Berman and T. Routtenberg, "Resource allocation and dithering of Bayesian parameter estimation using mixed-resolution data," *IEEE Trans. Signal Process.*, vol. 69, pp. 6148–6164, 2021.
- [12] Y. Ghasempour, M. K. Haider, and E. W. Knightly, "Decoupling beam steering and user selection for MU-MIMO 60-GHz WLANs," *IEEE/ACM Trans. Netw.*, vol. 26, no. 5, pp. 2390–2403, 2018.
- [13] G. C. Alexandropoulos, A. Clemente, S. Matos, R. Husbands, S. Ahearne, Q. Luo, V. Lain-Rubio, T. Kürner, and L. M. Pessoa, "Reconfigurable intelligent surfaces for THz: Signal processing and hardware design challenges," in *Proc. European Conf. Antennas Prop.*, Glasgow, Scotland, Mar. 2024.
- [14] S. Matos, Y. Ma, Q. Luo, J. Deurmeier, L. Lucci, P. Gavriilidis, A. Kiazadeh, V. Lain-Rubio, T. D. Phan, P. J. Soh, A. Clemente, L. M. Pessoa, and G. C. Alexandropoulos, "Reconfigurable intelligent surfaces for THz: Hardware impairments and switching technologies," in *Proc. Int. Conf. Electromagn. Adv. Appl. and IEEE-APS Topical Conf. Ant. Prop. Wireless Commun.*, Lisbon, Portugal, Sep. 2024.
- [15] S. S. Ioushua and Y. C. Eldar, "A family of hybrid analog–digital beamforming methods for massive MIMO systems," *IEEE Trans. Signal Process.*, vol. 67, no. 12, pp. 3243–3257, 2019.
- [16] N. Shlezinger, G. C. Alexandropoulos, M. F. Imani, Y. C. Eldar, and D. R. Smith, "Dynamic metasurface antennas for 6G extreme massive MIMO communications," *IEEE Wireless Commun.*, vol. 28, no. 2, pp. 106–113, 2021.
- [17] Z. Shao, R. Shen, W. Xia, Y. Ghasempour, K. Sengupta, and S. Rangan, "A hybrid antenna-metasurface architecture for mmWave and THz massive MIMO," in *Asilomar Conference on Signals, Systems, and Computers*. IEEE, 2023, pp. 1610–1616.
- [18] H. Chen and Y. Ghasempour, "Malicious mmwave reconfigurable surface: Eavesdropping through harmonic steering," in *International Workshop on Mobile Computing Systems and Applications*, 2022, pp. 54–60.
- [19] L. You, J. Xu, G. C. Alexandropoulos, J. Wang, W. Wang, and X. Gao, "Energy efficiency maximization of massive MIMO communications with dynamic metasurface antennas," *IEEE Trans. Wireless Commun.*, vol. 22, no. 1, pp. 393–407, 2023.
- [20] P. Gavriilidis and G. C. Alexandropoulos, "Near-field beam tracking with extremely massive dynamic metasurface antennas," *arXiv preprint arXiv:2406.01488*, 2024.
- [21] C. Huang, S. Hu, G. C. Alexandropoulos, A. Zappone, C. Yuen, R. Zhang, M. Di Renzo, and M. Debbah, "Holographic MIMO surfaces for 6G wireless networks: Opportunities, challenges, and trends," *IEEE Commun. Mag.*, vol. 27, no. 5, pp. 118–125, 2020.
- [22] T. Gong, P. Gavriilidis, R. Ji, C. Huang, G. C. Alexandropoulos, L. Wei, M. Debbah, H. V. Poor, and C. Yuen, "Holographic MIMO communications: Theoretical foundations, enabling technologies, and future directions," *IEEE Commun. Surveys & Tuts.*, vol. 26, no. 1, pp. 196–257, 2024.
- [23] E. Ghaderi, A. S. Ramani, A. A. Rahimi, D. Heo, S. Shekhar, and S. Gupta, "An integrated discrete-time delay-compensating technique for large-array beamformers," *IEEE Trans. Circuits Syst. I*, vol. 66, no. 9, pp. 3296–3306, 2019.

- [24] B. Zhai, Y. Zhu, A. Tang, and X. Wang, "THzPrism: Frequency-based beam spreading for terahertz communication systems," *IEEE Wireless Commun. Lett.*, vol. 9, no. 6, pp. 897–900, 2020.
- [25] B. Zhai, A. Tang, C. Peng, and X. Wang, "SS-OFDMA: Spatial-spread orthogonal frequency division multiple access for terahertz networks," *IEEE J. Sel. Areas Commun.*, vol. 39, no. 6, pp. 1678–1692, 2021.
- [26] L. Dai, J. Tan, Z. Chen, and H. V. Poor, "Delay-phase precoding for wideband THz massive MIMO," *IEEE Transactions on Wireless Communications*, vol. 21, no. 9, pp. 7271–7286, 2022.
- [27] D. Q. Nguyen and T. Kim, "Joint delay-phase precoding under true-time delay constraints in wideband sub-THz hybrid massive MIMO systems," *IEEE Trans. Commun.*, 2024.
- [28] H. Do, N. Lee, R. W. Heath, and A. Lozano, "Hybrid arrays: How many RF chains are required to prevent beam squint?" *IEEE Trans. Wireless Commun.*, 2024.
- [29] R. Li, H. Yan, and D. Cabric, "Rainbow-link: Beam-alignment-free and grant-free mmW multiple access using true-time-delay array," *IEEE J. Sel. Areas Commun.*, vol. 40, no. 5, pp. 1692–1705, 2022.
- [30] V. V. Ratnam, J. Mo, A. Alammouri, B. L. Ng, J. Zhang, and A. F. Molisch, "Joint phase-time arrays: A paradigm for frequency-dependent analog beamforming in 6G," *IEEE Access*, vol. 10, pp. 73 364–73 377, 2022.
- [31] E. Vlachos, A. Kaushik, Y. C. Eldar, and G. C. Alexandropoulos, "Time-domain channel estimation for extremely large MIMO THz communication systems under dual-wideband fading conditions," *arXiv preprint arXiv:2310.14745*, 2020.
- [32] A. A. Oliner, D. R. Jackson, and J. Volakis, "Leaky-wave antennas," *Antenna engineering handbook*, vol. 4, p. 12, 2007.
- [33] H. Guerboukha, R. Shrestha, J. Neronha, Z. Fang, and D. M. Mittleman, "Conformal leaky-wave antennas for wireless terahertz communications," *Communications Engineering*, vol. 2, no. 1, p. 17, 2023.
- [34] O. Zetterstrom, E. Pucci, P. Padilla, L. Wang, and O. Quevedo-Teruel, "Low-dispersive leaky-wave antennas for mmWave point-to-point high-throughput communications," *IEEE Trans. Antennas Propag.*, vol. 68, no. 3, pp. 1322–1331, 2019.
- [35] Y. Ghasempour, C.-Y. Yeh, R. Shrestha, D. Mittleman, and E. Knightly, "Single shot single antenna path discovery in THz networks," in *International Conference on Mobile Computing and Networking*, 2020.
- [36] Y. Ghasempour, R. Shrestha, A. Charous, E. Knightly, and D. M. Mittleman, "Single-shot link discovery for terahertz wireless networks," *Nature communications*, vol. 11, no. 1, p. 2017, 2020.
- [37] A. Kludze and Y. Ghasempour, "{LeakyScatter}: A {Frequency-Agile} directional backscatter network above 100 {GHz}," in *USENIX Symposium on Networked Systems Design and Implementation (NSDI 23)*, 2023, pp. 375–388.
- [38] N. J. Karl, R. W. McKinney, Y. Monnai, R. Mendis, and D. M. Mittleman, "Frequency-division multiplexing in the terahertz range using a leaky-wave antenna," *Nature Photonics*, vol. 9, no. 11, pp. 717–720, 2015.
- [39] H. Rahmani, D. Shetty, M. Wagih, Y. Ghasempour, V. Palazzi, N. B. Carvalho, R. Correia, A. Costanzo, D. Vital, F. Alimenti *et al.*, "Next-generation IoT devices: Sustainable eco-friendly manufacturing, energy harvesting, and wireless connectivity," *IEEE Journal of Microwaves*, vol. 3, no. 1, pp. 237–255, 2023.
- [40] Y. Ghasempour, C.-Y. Yeh, R. Shrestha, Y. Amarasinghe, D. Mittleman, and E. W. Knightly, "LeakyTrack: Non-coherent single-antenna nodal and environmental mobility tracking with a leaky-wave antenna," in *Conference on Embedded Networked Sensor Systems (SenSys)*, 2020.
- [41] A. Kludze, R. Shrestha, C. Miftah, E. Knightly, D. Mittleman, and Y. Ghasempour, "Quasi-optical 3D localization using asymmetric signatures above 100 GHz," in *International Conference on Mobile Computing And Networking*, 2022, pp. 120–132.
- [42] C.-Y. Yeh, Y. Ghasempour, Y. Amarasinghe, D. M. Mittleman, and E. W. Knightly, "Security and angle-frequency coupling in terahertz WLANs," *IEEE/ACM Trans. Netw.*, vol. 32, no. 2, pp. 1524–1539, 2024.
- [43] V. Boljanovic, H. Yan, C.-C. Lin, S. Mohapatra, D. Heo, S. Gupta, and D. Cabric, "True-time-delay arrays for fast beam training in wideband millimeter-wave systems," *IEEE Trans. Circuits Syst. I*, vol. 68, no. 4, pp. 1727–1739, 2021.
- [44] H. Saeidi, S. Venkatesh, X. Lu, and K. Sengupta, "22.1 THz Prism: One-shot simultaneous multi-node angular localization using spectrum-to-space mapping with 360-to-400GHz broadband transceiver and dual-port integrated leaky-wave antennas," in *IEEE International Solid-State Circuits Conference (ISSCC)*, vol. 64, 2021, pp. 314–316.
- [45] A. Moreira, P. Prats-Iraola, M. Younis, G. Krieger, I. Hajnsek, and K. P. Papathanassiou, "A tutorial on synthetic aperture radar," *IEEE Geosci. Remote Sens. Mag.*, vol. 1, no. 1, pp. 6–43, 2013.
- [46] C. Han, Y. Wang, Y. Li, Y. Chen, N. A. Abbasi, T. Kürner, and A. F. Molisch, "Terahertz wireless channels: A holistic survey on measurement, modeling, and analysis," *IEEE Commun. Surveys Tuts.*, vol. 24, no. 3, pp. 1670–1707, 2022.
- [47] D. Tse and P. Viswanath, *Fundamentals of wireless communication*. Cambridge university press, 2005.
- [48] Z. Shen, R. Chen, J. G. Andrews, R. W. Heath, and B. L. Evans, "Sum capacity of multiuser MIMO broadcast channels with block diagonalization," *IEEE Trans. Wireless Commun.*, vol. 6, no. 6, pp. 2040–2045, 2007.
- [49] P. He, L. Zhao, S. Zhou, and Z. Niu, "Water-filling: A geometric approach and its application to solve generalized radio resource allocation problems," *IEEE Trans. Wireless Commun.*, vol. 12, no. 7, pp. 3637–3647, 2013.
- [50] C. Xing, Y. Jing, S. Wang, S. Ma, and H. V. Poor, "New viewpoint and algorithms for water-filling solutions in wireless communications," *IEEE Trans. Signal Process.*, vol. 68, pp. 1618–1634, 2020.
- [51] V. Boljanovic and D. Cabric, "Joint millimeter-wave AoD and AoA estimation using one OFDM symbol and frequency-dependent beams," in *IEEE International Conference on Acoustics, Speech and Signal Processing (ICASSP)*, 2023.
- [52] L. Brandenburg and A. Wyner, "Capacity of the Gaussian channel with memory: The multivariate case," *Bell System Technical Journal*, vol. 53, no. 5, pp. 745–778, 1974.
- [53] H. Zhang, N. Shlezinger, F. Guidi, D. Dardari, M. F. Imani, and Y. C. Eldar, "Beam focusing for near-field multiuser MIMO communications," *IEEE Trans. Wireless Commun.*, vol. 21, no. 9, pp. 7476–7490, 2022.